

ESTIMATING THE AVERAGE SIZE OF FIBER/MATRIX INTERFACE CRACKS IN UD AND CROSS-PLY LAMINATES

L. Di Stasio^{1,2}, J. Varna¹, Z. Ayadi²

¹Division of Materials Science, Luleå University of Technology, Luleå, Sweden

²EEIGM & IJL, Université de Lorraine, Nancy, France

7th ECCOMAS Thematic Conference on the Mechanical Response of Composites
Girona (ES) - September 18-20, 2019



Education and Culture

Erasmus Mundus

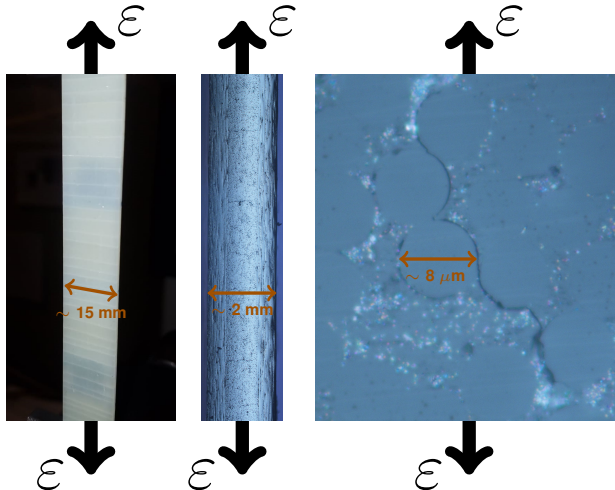


Outline

- Transverse Cracks Initiation in FRPC
- Modeling
- Debond Initiation
- Debond Propagation
- Conclusions

TRANSVERSE CRACKS INITIATION IN FRPC

Micromechanics of Initiation: Transverse Tensile Loading



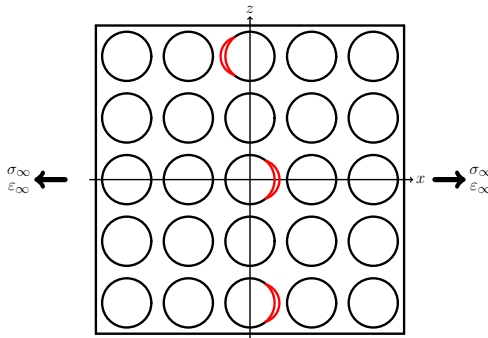
Left:
front view of [0, 90₂]_S,
visual inspection.

Center:
edge view of [0, 90]_S,
optical microscope.

Right:
edge view of [0, 90]_S,
optical microscope.

Micromechanics of Initiation: Transverse Tensile Loading

Stage 1: isolated debonds



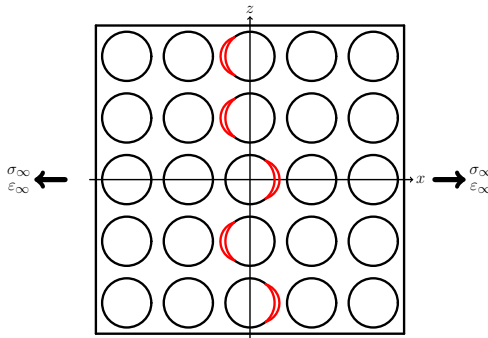
Bailey et al., P. Roy. Soc. A-Math. Phys. **366** (1727), 1979.

Bailey et al., J. Mater. Sci. **16** (3), 1981.

Zhang et al., Compos. Part A-Appl. S. **28** (4), 1997.

Micromechanics of Initiation: Transverse Tensile Loading

Stage 2: consecutive debonds



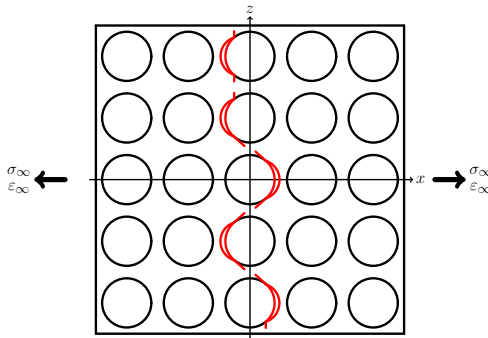
Bailey et al., P. Roy. Soc. A-Math. Phys. **366** (1727), 1979.

Bailey et al., J. Mater. Sci. **16** (3), 1981.

Zhang et al., Compos. Part A-Appl. S. **28** (4), 1997.

Micromechanics of Initiation: Transverse Tensile Loading

Stage 3: kinking



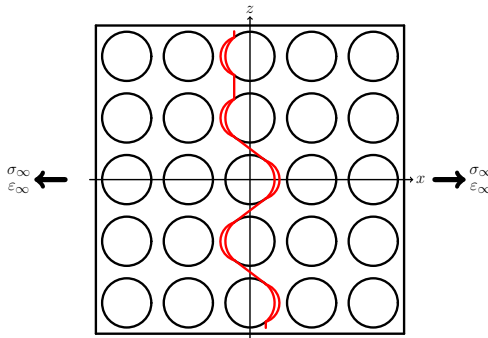
Bailey et al., P. Roy. Soc. A-Math. Phys. **366** (1727), 1979.

Bailey et al., J. Mater. Sci. **16** (3), 1981.

Zhang et al., Compos. Part A-Appl. S. **28** (4), 1997.

Micromechanics of Initiation: Transverse Tensile Loading

Stage 4: coalescence



Bailey et al., P. Roy. Soc. A-Math. Phys. **366** (1727), 1979.

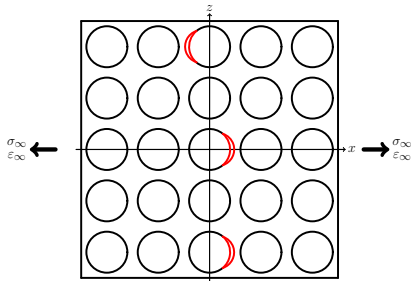
Bailey et al., J. Mater. Sci. **16** (3), 1981.

Zhang et al., Compos. Part A-Appl. S. **28** (4), 1997.

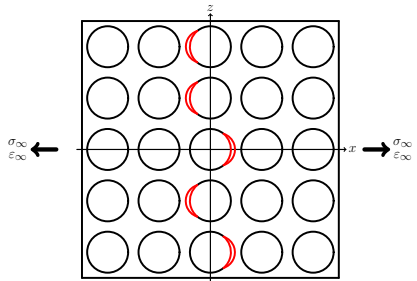
Objective of the Study

Can we talk about a ply-thickness effect for the fiber-matrix interface crack?

Stage 1: isolated debonds

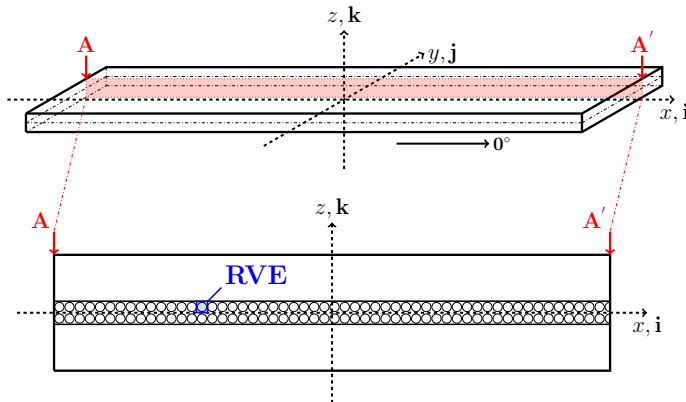


Stage 2: consecutive debonds



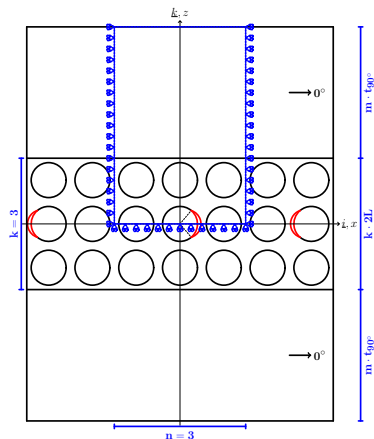
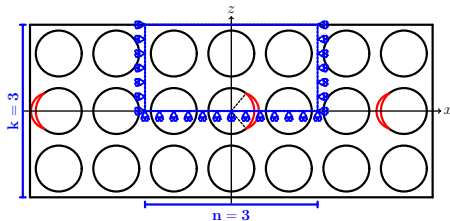
MODELING

Geometry

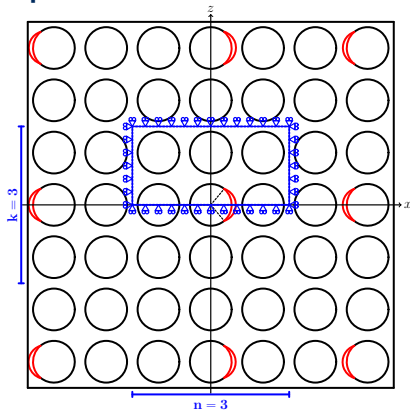


- $L, W \gg t$
- $L, W \rightarrow \infty$
- Square packing
- $L_d \gg \Delta\theta_d$
- 2D RVE

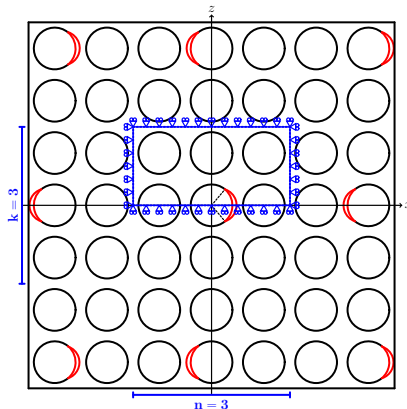
Representative Volume Elements



Representative Volume Elements

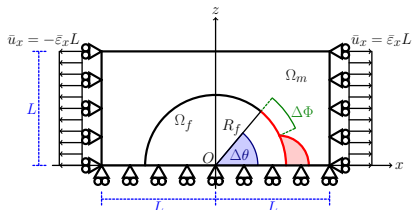


$n \times k - \text{symm}$



$n \times k - \text{asymm}$

Assumptions

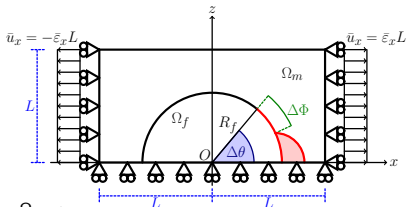


$$R_f = 1 \text{ } [\mu\text{m}] \quad L = \frac{R_f}{2} \sqrt{\frac{\pi}{V_f}}$$

- Linear elastic, homogeneous materials
- Concentric Cylinders Assembly with Self-Consistent Shear Model for UD
- Plane strain
- Frictionless contact interaction
- Symmetric w.r.t. x-axis
- Coupling of x-displacements on left and right side (repeating unit cell)
- Applied uniaxial tensile strain $\bar{\epsilon}_x = 1\%$
- $V_f = 60\%$

| Material | V_f [%] | E_L [GPa] | E_T [GPa] | μ_{LT} [GPa] | ν_{LT} [-] | ν_{TT} [-] |
|-------------|-----------|-------------|-------------|------------------|----------------|----------------|
| Glass fiber | - | 70.0 | 70.0 | 29.2 | 0.2 | 0.2 |
| Epoxy | - | 3.5 | 3.5 | 1.25 | 0.4 | 0.4 |
| UD | 60.0 | 43.442 | 13.714 | 4.315 | 0.273 | 0.465 |

Solution



in $\Omega_f, \Omega_m, \Omega_{UD}$:

$$\frac{\partial^2 \varepsilon_{xx}}{\partial z^2} + \frac{\partial^2 \varepsilon_{zz}}{\partial x^2} = \frac{\partial^2 \gamma_{zx}}{\partial x \partial z} \quad \text{for } 0^\circ \leq \alpha \leq \Delta\theta, \Delta\theta \neq 0^\circ :$$

$$(\vec{u}_m(R_f, \alpha) - \vec{u}_f(R_f, \alpha)) \cdot \vec{n}_\alpha \geq 0$$

$$\varepsilon_y = \gamma_{xy} = \gamma_{yz} = 0 \quad \text{for } \Delta\theta \leq \alpha \leq 180^\circ :$$

$$\frac{\partial \sigma_{xx}}{\partial x} + \frac{\partial \tau_{zx}}{\partial z} = 0 \quad \vec{u}_m(R_f, \alpha) - \vec{u}_f(R_f, \alpha) = 0$$

$$\frac{\partial \tau_{zx}}{\partial x} + \frac{\partial \sigma_{zz}}{\partial z} = 0 \quad \sigma_{ij} = E_{ijkl} \varepsilon_{kl} + BC$$

$$\sigma_{yy} = \nu (\sigma_{xx} + \sigma_{zz})$$

$$\forall \Delta\theta \neq 0^\circ$$

→ oscillating singularity

$$\sigma \sim r^{-\frac{1}{2}} \sin(\varepsilon \log r), \quad V_f \rightarrow 0$$

$$\varepsilon = \frac{1}{2\pi} \log \left(\frac{1 - \beta}{1 + \beta} \right)$$

$$\beta = \frac{\mu_2 (\kappa_1 - 1) - \mu_1 (\kappa_2 - 1)}{\mu_2 (\kappa_1 + 1) + \mu_1 (\kappa_2 + 1)}$$

→ receding contact

$$\rightarrow \frac{G(R_{f,2})}{G(R_{f,1})} = \frac{R_{f,2}}{R_{f,1}}, \quad \frac{G(\bar{\varepsilon}_{x,2})}{G(\bar{\varepsilon}_{x,1})} = \frac{\bar{\varepsilon}_{x,2}^2}{\bar{\varepsilon}_{x,1}^2}$$

→ FEM + LEFM (VCCT)

→ regular mesh of quadrilaterals at the crack tip:

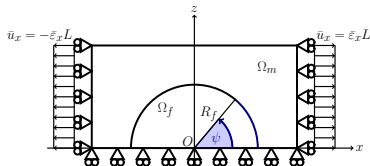
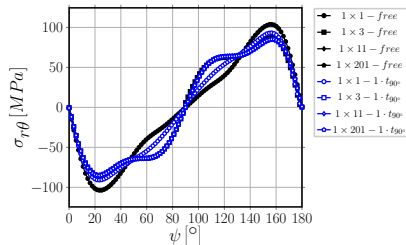
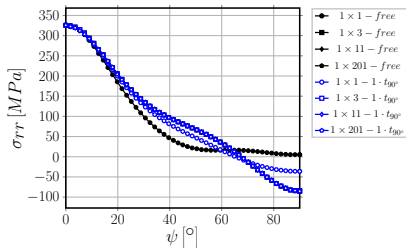
$$- AR \sim 1, \quad \delta = 0.05^\circ$$

$$\forall \Delta\theta$$

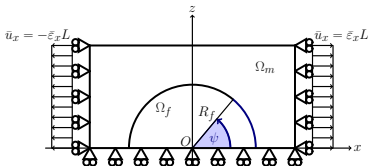
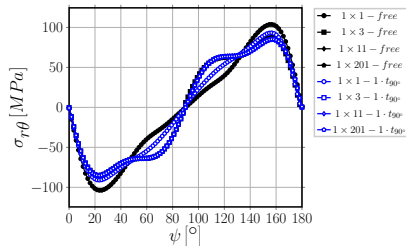
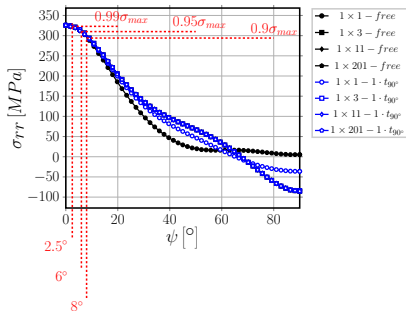
→ 2nd order shape functions

➤ DEBOND INITIATION

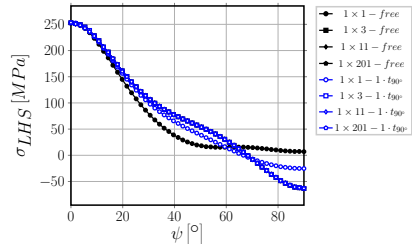
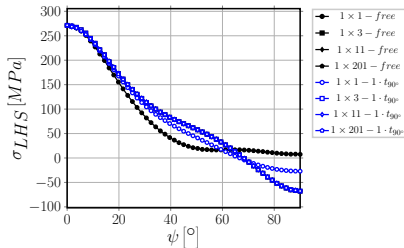
σ_{rr} VS $\tau_{r\theta}$: radial stress vs tangential shear at the interface



σ_{rr} VS $\tau_{r\theta}$: radial stress vs tangential shear at the interface

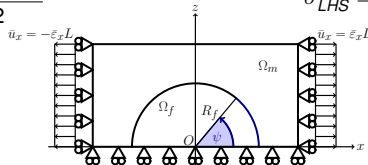


σ_{LHS} : local hydrostatic stress at the interface

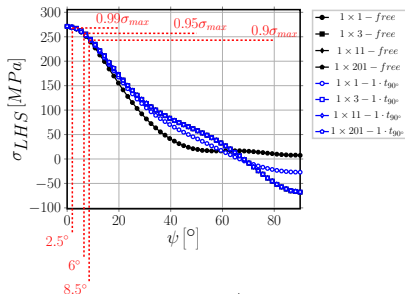


$$\sigma_{LHS}^{2D} = \frac{\sigma_{rr} + \sigma_{\theta\theta}}{2}$$

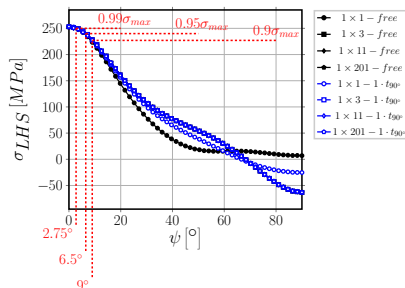
$$\sigma_{LHS}^{3D} = \frac{\sigma_{rr} + \sigma_{\theta\theta} + \sigma_{yy}}{3}$$



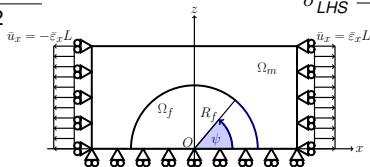
σ_{LHS} : local hydrostatic stress at the interface



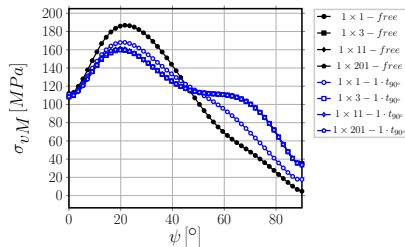
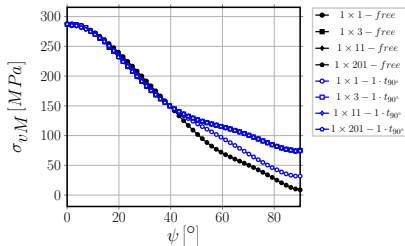
$$\sigma_{LHS}^{2D} = \frac{\sigma_{rr} + \sigma_{\theta\theta}}{2}$$



$$\sigma_{LHS}^{3D} = \frac{\sigma_{rr} + \sigma_{\theta\theta} + \sigma_{yy}}{3}$$

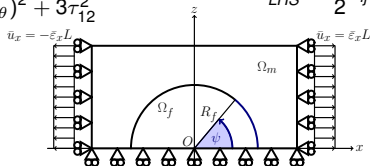


σ_{vM} : von Mises stress at the interface

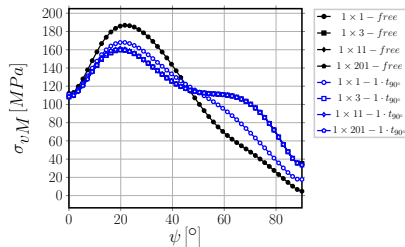
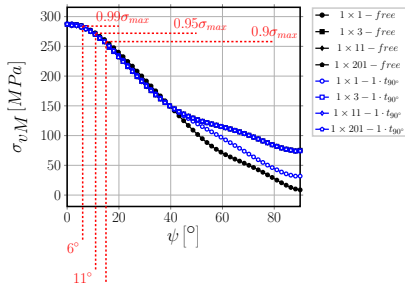


$$\sigma_{vM}^{2D} = \sqrt{(\sigma_{rr} - \sigma_{\theta\theta})^2 + 3\tau_{12}^2}$$

$$\sigma_{LHS}^{3D} = \frac{3}{2} s_{ij} s_{ij} \quad s_{ij} = \sigma_{ij} - \frac{1}{3} \sigma_{kk} \delta_{ij}$$

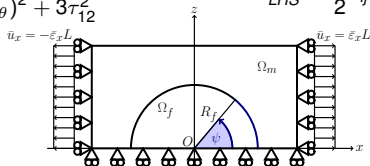


σ_{vM} : von Mises stress at the interface

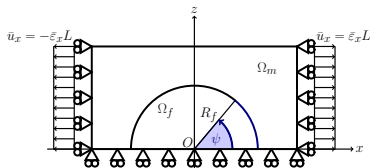
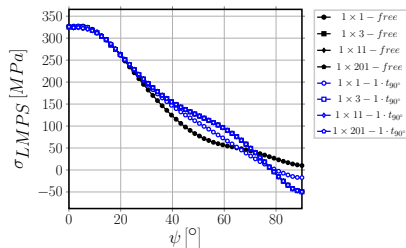
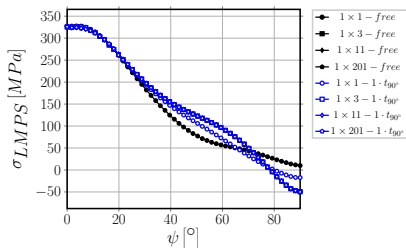


$$\sigma_{vM}^{2D} = \sqrt{(\sigma_{rr} - \sigma_{\theta\theta})^2 + 3\tau_{12}^2}$$

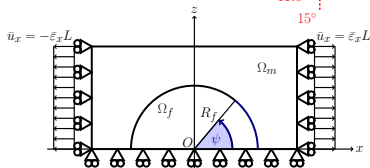
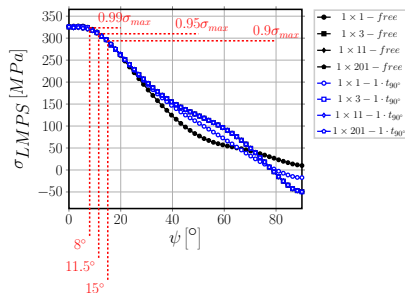
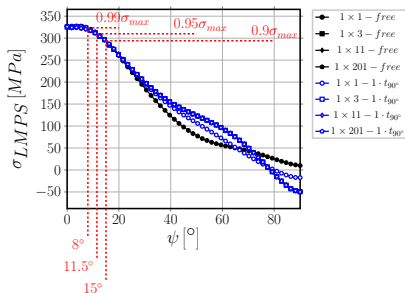
$$\sigma_{LHS}^{3D} = \frac{3}{2} s_{ij} s_{ij} \quad s_{ij} = \sigma_{ij} - \frac{1}{3} \sigma_{kk} \delta_{ij}$$



σ_I : maximum principal stress at the interface



σ_I : maximum principal stress at the interface



Observations & Conclusions

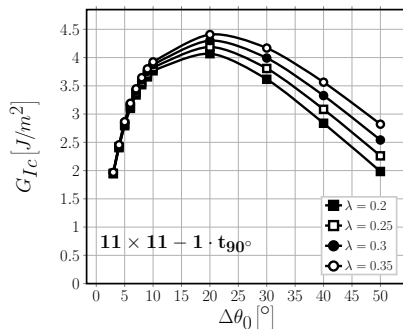
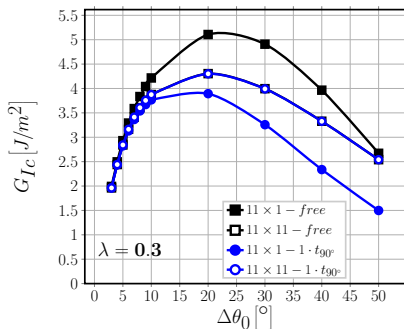
- For all stresses analyzed, no significant difference is present between the different RUCs for $\psi \leq 10^\circ$;
- for all stresses analyzed, no difference can be observed by increasing k when $k \geq 3$;
- for all stresses analyzed, no difference can be observed between $1 \times k - free$ and $1 \times k - 1 \cdot t_{90^\circ}$ for $k \geq 3$;
- σ_{rr} , $\sigma_{LHS,2D}$, $\sigma_{LHS,3D}$, $\sigma_{VM,2D}$, $\sigma_{LMPS,2D}$ and $\sigma_{LMPS,3D}$ all reach their peak value at 0° and 180° and decrease to 99% the peak value between 2° and 8° , to 95% the peak value between 6° and 12° and to 90% the peak value between 8° and 15° from the occurrence of the maximum.

It seems reasonable to conclude that...

...a stress-based criterion would predict, irrespectively of the specific criterion chosen, the onset of an interface crack at 0° or 180° with an initial size at least comprised in the range $2^\circ - 8^\circ$ (1% margin) and likely in the range $6^\circ - 12^\circ$ (5% margin).

DEBOND PROPAGATION

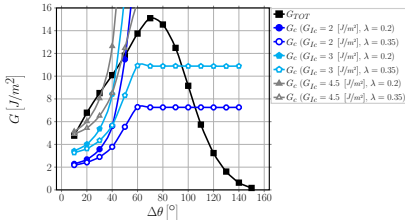
Estimation of G_{Ic}



$$G_{Ic} = \frac{G_c}{1 + \tan^2((1 - \lambda)\Psi_G)} \Big|_{G_c=G_{TOT}(\Delta\theta_0)}, \quad \Psi_G = \tan^{-1} \left(\sqrt{\frac{G_{II}}{G_I}} \right) \Big|_{\Delta\theta_0}$$

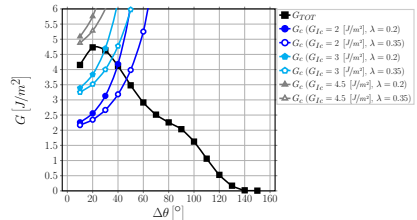
Estimation of $\Delta\theta_{max}$

$21 \times 1 - free$



$\Delta\theta_{max} \in (30^\circ - 105^\circ)$

$21 \times 1 - 1 \cdot t_{90^\circ}$

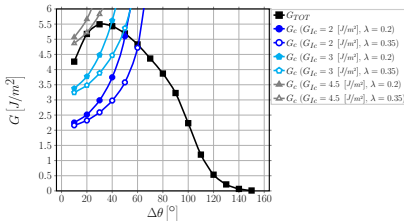


$\Delta\theta_{max} \in (30^\circ - 50^\circ)$

$$G_{TOT}(\Delta\theta) > G_c = G_{Ic} \left(1 + \tan^2((1 - \lambda) \Psi_G) \right), \quad \Psi_G = \tan^{-1} \left(\sqrt{\frac{G_{II}}{G_I}} \right) \Big|_{\Delta\theta}$$

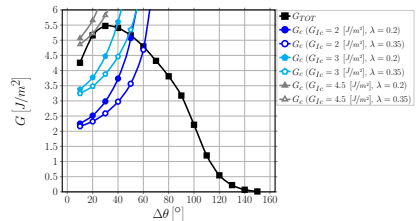
Estimation of $\Delta\theta_{max}$

$21 \times 3 - free$



$\Delta\theta_{max} \in (40^\circ - 60^\circ)$

$21 \times 3 - 1 \cdot t_{90^\circ}$

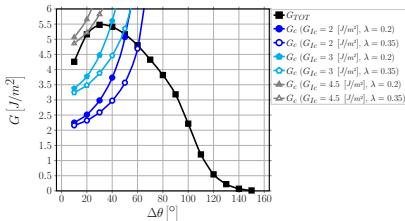


$\Delta\theta_{max} \in (40^\circ - 60^\circ)$

$$G_{TOT}(\Delta\theta) > G_c = G_{Ic} \left(1 + \tan^2((1 - \lambda) \Psi_G) \right), \quad \Psi_G = \tan^{-1} \left(\sqrt{\frac{G_{II}}{G_I}} \right) \Big|_{\Delta\theta}$$

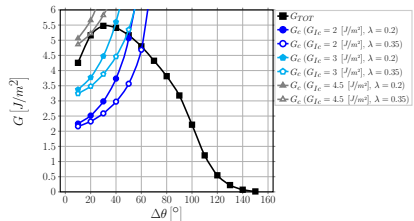
Estimation of $\Delta\theta_{max}$

$21 \times 21 - free$



$$\Delta\theta_{max} \in (40^\circ - 60^\circ)$$

$21 \times 21 - 1 \cdot t_{90^\circ}$

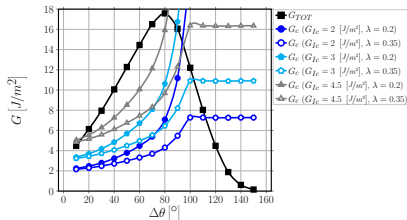


$$\Delta\theta_{max} \in (40^\circ - 60^\circ)$$

$$G_{TOT}(\Delta\theta) > G_c = G_{Ic} \left(1 + \tan^2((1 - \lambda) \Psi_G) \right), \quad \Psi_G = \tan^{-1} \left(\sqrt{\frac{G_{II}}{G_I}} \right) \Big|_{\Delta\theta}$$

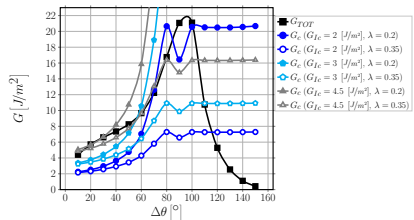
Estimation of $\Delta\theta_{max}$

21 × 21 – *symm*



$\Delta\theta_{max} \in (80^\circ - 110^\circ)$

21 × 21 – *asymm*



$\Delta\theta_{max} \in (55^\circ - 115^\circ)$

$$G_{TOT}(\Delta\theta) > G_c = G_{Ic} \left(1 + \tan^2((1 - \lambda) \Psi_G) \right), \quad \Psi_G = \tan^{-1} \left(\sqrt{\frac{G_{II}}{G_I}} \right) \Big|_{\Delta\theta}$$

Observations & Conclusions

- The effect of the presence of the 0° layer is to reduce the maximum size of debonds;
- however, the estimated debond size is the same for $n \times k - free$ and $n \times k - 1 \cdot t_{90^\circ}$ for $k \geq 3$;
- the presence of a debond on the neighboring fiber in the vertical direction ($21 \times 1 - coupling$ and $21 \times 1 - asymm$) favors instead the growth of larger debonds;
- the largest size is achieved when debonds are on opposite sides of consecutive fibers.

Estimated debond size range in cross-ply ($n \times k - 1 \cdot t_{90^\circ}$)

$40^\circ - 60^\circ$

Measured debond size range in cross-ply (Correa et al., Compos. Sci. Technol. 155 (213-220), 2018)

$21.4^\circ - 89.2^\circ$, average 49.3° , standard deviation of 11.7°
 63% of measurements in $40^\circ - 60^\circ$ range

CONCLUSIONS

Conclusions

- A stress criterion for initiation would likely predict, irrespectively of which criterion from those proposed in the literature is chosen, the onset of a debond at 0° or 180° with a semi-aperture $\Delta\theta_0$ in the range $2^\circ - 12^\circ$, corresponding to a margin of 5% on the satisfaction of the criterion.
- Assuming that debond propagation occurs unstably immediately after debond onset at the same level of global applied strain $\bar{\epsilon}_x$, it is possible to evaluate the parameter G_{lc} in the expression of the critical ERR and with it to estimate the range of expected maximum debond size.
- The prediction for a cross-ply laminate (models $n \times k - 1 \cdot t_{90^\circ}$, $k \geq 3$) agrees well with the debond size distribution in $[0_3^\circ, 90_3^\circ]_S$ estimated in *Correa et al., Compos. Sci. Technol.* **155** (213-220), 2018 through microscopic observations.

Thank you for listening today!

